Nuclear Inst. and Methods in Physics Research, A 990 (2021) 164979

Contents lists available at ScienceDirect

Nuclear Inst. and Methods in Physics Research, A

journal homepage: www.elsevier.com/locate/nima

Error characterization and calibration of real-time magnetic field measurement systems

Christian Grech [a,b,*], Maria Amodeo [c,a], Anthony Beaumont [a], Marco Buzio [a], Vincenzo Di Capua [a,d], David Giloteaux [a], Nicholas Sammut [a,b], Joseph Vella Wallbank [a,b]

[a] CERN, European Organization for Nuclear Research, 1211 Geneva, Switzerland
[b] Università ta' Malta, Msida MSD 2080, Malta
[c] Politecnico di Torino, Turin, 10129, Italy
[d] Università degli Studi di Napoli Federico II, Naples, Italy

ARTICLE INFO

Keywords:
B-train
Calibration
Field marker
Ferrimagnetic resonance
Induction coil
Nuclear magnetic resonance
Real-time magnetic measurement
Synchrotron

ABSTRACT

In synchrotrons at the European Organization for Nuclear Research (CERN), magnetic measurement systems known as B-trains measure the magnetic field in the main bending magnets in real-time, and transmit this signal for the control of the synchrotron's RF accelerating cavities, magnet power converter and beam monitoring systems. This work presents an assessment of the capabilities and performance of the new FIRESTORM (Field In REal-time STreaming from Online Reference Magnets) system as part of the first phase of commissioning. A short summary of the architecture of the measurement system is provided first, followed by the definition of an error model which can be used to characterize random and systematic errors separately. We present a procedure for the metrological calibration and qualification of the B-trains, including an experimental evaluation of the different error sources for the four new systems being commissioned in the Proton Synchrotron Booster (PSB), Low Energy Ion Ring (LEIR), Proton Synchrotron (PS) and the Extra Low ENergy Antiproton (ELENA) ring. In particular, we discuss a method to calibrate systematic gain and offset errors based on the RF cavity frequency offset needed to center the beam on its theoretical orbit.

1. Introduction

In particle synchrotrons, the vertical magnetic field produced by the bending magnets is used to guide charged particles along a closed horizontal orbit, determined by the equilibrium of the centrifugal force and the Lorentz force. Knowledge of the instantaneous value of the magnetic field is essential, especially for the control of the radio-frequency (RF) cavity. For this purpose, a direct magnetic field measurement inside a reference magnet representing the average of the bending units is often used [1]. At CERN, this is known as a B-train system. Similar systems are also implemented at the Brookhaven National Laboratory [2] and at several hadrontherapy facilities including the National Centre of Oncological Hadrontherapy (CNAO) [3,4], MedAustron [5,6] and the Heidelberg Ion-Beam Therapy Center (HIT) [7,8].

Fig. 1 shows the synchrotrons that form part of the CERN accelerator complex. Six machines make use of B-train systems: the Low Energy Ion Ring (LEIR), the Proton Synchrotron Booster (PSB), the Proton Synchrotron (PS) [9], the Antiproton Decelerator (AD), the Extra Low Energy Antiproton (ELENA) [10], and the Super Proton Synchrotron (SPS) [11,12]. The PSB, LEIR, PS and SPS form part of the Large Hadron Collider (LHC) injector chain. The PSB consists of four superimposed rings accelerating in parallel protons injected from Linac 2 at an energy level of 50 MeV up to a level of 1.4 GeV, to be extracted towards the PS (injection energy will be increased in the second half of 2020, when Linac 4 will come online). The LEIR ring accelerates heavy ions injected from Linac 3 from the level of 4.2 MeV/nucleon up to 72 MeV/nucleon, when they are extracted to the PS ring. The PS can receive either protons or heavy ions, and in this work, the proton case will be considered. These are accelerated up to 26 GeV and subsequently sent to the SPS and accelerated to 450 GeV to the LHC. On the other hand, the ELENA synchrotron decelerates antiprotons provided by the AD from 5.3 MeV down to 100 keV. Hence, the machine operates at an unusually low energy [13], making the beam more sensitive to field errors.

As part of a site-wide, long-term consolidation project, all the legacy B-train systems at CERN (some in operation since two decades) are in the process of being replaced with upgraded electronics, software and sensors. The new B-train system is referred to as FIRESTORM (Field In REal-time STreaming from Online Reference Magnets). The first four systems completed, i.e. those in the LEIR, PSB, PS and ELENA rings, were tested extensively during the last operating phase of the complex

* Corresponding author at: Università ta' Malta, Msida MSD 2080, Malta.
E-mail address: christian.grech.12@um.edu.mt (C. Grech).

https://doi.org/10.1016/j.nima.2020.164979
Received 30 April 2020; Received in revised form 1 October 2020; Accepted 17 December 2020
Available online 26 December 2020

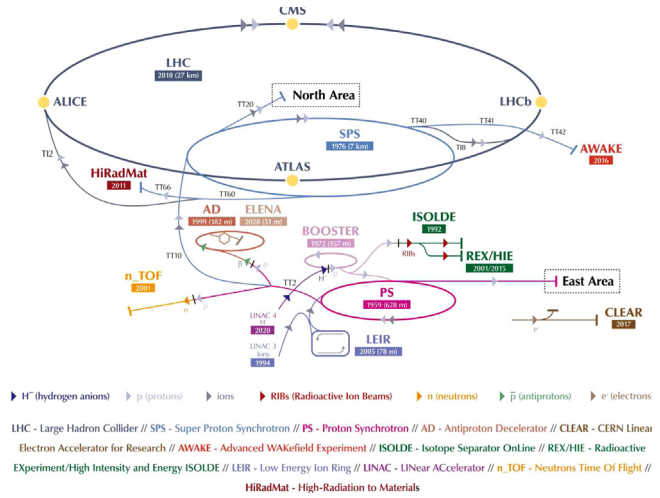

Fig. 1. The CERN accelerator complex in 2019 [14].

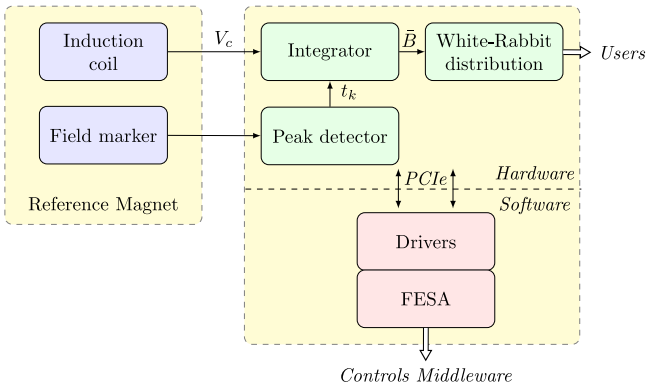

Fig. 2. Schematic representation of B-train system.

in 2018, before a three-year shutdown for maintenance and upgrades. The SPS system is being completed in due time for the 2021's restart, while the AD system requires only to broadcast the magnetic cycle computed from the beam momentum, no actual measurement being done.

This work is mainly concerned with the presentation and analysis of the results of these tests, assessing the metrological performance and reliability of the new B-trains. The paper is structured as follows: Section 2 contains a general description of the B-train measurement systems, while in Section 3 the measurement error model is defined. Random and systematic error components are discussed in detail in Sections 4 and 5 respectively, including methods to verify the performance of the systems and calibrate them using beam-based measurements. The conclusions are summarized in Section 6.

2. Measurement system overview

2.1. Measurement model

B-trains are designed to provide the average field $\bar{B}(t)$ over the bending magnets in the ring. The measurement is based upon a fixed induction coil [15] inserted in the gap of a reference magnet, and it can be expressed by (1):

$$\bar{B}(t) = B_{\mathrm{m}} + \frac{1}{A_c}\int_{t_k}^{t} V_c(\tau)\,d\tau,\ t_k \le t < t_{k+1} \tag{1}$$

where V_{c} is the voltage induced in the coil, A_{c} is its effective area and B_{m} is the integration constant derived from an additional sensor called a *field marker*. The field marker operates by emitting a trigger whenever the field crosses the pre-determined level B_{m}, thus periodically restarting the integration at $t = t_k$, with $k = 1, 2, \ldots$. The typical interval between restarts is of the order of a few seconds, with the main exception of ELENA where cycles may be much longer. While the system can in principle accept multiple field markers working at different levels, in this work we shall apply only one marker trigger at the start of each magnetic cycle, so that k can in practice be considered as a cycle index.

2.2. Hardware and software architecture

In general, each FIRESTORM measurement system includes two identical acquisition chains, one operational and one spare. The overall architecture of a chain can be seen in Fig. 2. Each chain is based on a rectangular induction coil, that ideally should be elongated and shaped so as to capture the totality of the time-varying dipole field in a reference magnet's gap. When that is not possible, due to lack of space, a shorter coil is used instead and its effective area is scaled accordingly. The coil output voltage is first conditioned by an anti-aliasing RC filter and then is acquired by an 18-bit, 2-MHz analog-to-digital converter (ADC), to be finally integrated numerically in a field-programmable gate array (FPGA) [16,17]. These electronic components are integrated onto a PCIe carrier with an FPGA mezzanine card (FMC). The firmware includes a sophisticated correction mechanism to minimize input voltage offset. Nevertheless, integrator drift remains one of the dominant error sources, as discussed in Section 4.1.

In addition to the induction coil, field marker sensors placed in the magnet's gap generate a trigger signal when the magnetic field crosses a specific preset threshold. Nuclear magnetic resonance (NMR) probes [10,11,18] or ferrimagnetic resonance (FMR) probes [10,19] are used at CERN as a reference standard for the measurement. The working point of each probe is set by a fixed radio frequency signal that is proportional to the effective gyromagnetic ratio of the sample, i.e., approximately 42 MHz/T for the proton NMR and approximately 28 GHz/T for the electrons in the FMR samples. The precise gyromagnetic ratio of FMR samples depends upon many variables such as their chemical composition, their orientation respect to the field and the temperature, and is the object of a separate calibration [19]. A dedicated trigger generator FMC, amplifies and digitizes the signal generated from each field marker sensor. By using a differential algorithm, the resonance peak of the field marker output is found and a TTL trigger is generated.

The new B-trains make use of the CERN-developed White Rabbit fieldbus [20] to transmit the average magnetic field values to the different users. The transmission system distributes digitally the absolute values of the magnetic field, along with its time derivative, in nanosecond-synchronized Ethernet frames at a rate up to 250 kHz. All electronics are operated by means of software based on a real-time, distributed C++ framework called FESA (Front End Software Architecture), developed at CERN to manage and control all accelerator subsystems [21]. A FESA executable is carried out in a Front-End Computer (FEC) in every chain, where it is used for remote configuration, diagnostics and data broadcasting. The measurement data used in the present work were obtained via FESA at a sample rate up to 10 kHz.

2.3. Experimental setups

In this section we discuss the differences between the setups tested in the four different machines. The magnetic cycles chosen for the test are presented in Fig. 3 and their parameters are summarized in Table 1. In general, these cycles were interspersed within many other different ones as a part of repeated sequences ("supercycles"), determined according to the needs of different physics users and to the schedule of the

Table 1
Magnetic cycle properties.

Parameter	Symbol	Unit	PSB	LEIR[a]	PS[b]	ELENA[c]
Injection time	t_{inj}	ms	275	245	170	2727
Extraction time	t_{ex}	ms	805	2880	1650	30 000
Nominal field at t_{inj}	$B(t_{inj})$	mT	125	272	101	359
Nominal field at t_{ex}	$B(t_{ex})$	mT	861	1148	1255	49
Excitation current at t_{inj}	$I(t_{inj})$	A	580	769	404	276
Excitation current at t_{ex}	$I(t_{ex})$	A	4014	3290	5372	38
Field marker trigger time	t_1	ms	197	117.8	84.2[d]	2315
Field marker level	B_m	mT	110.8	251.2	49.5[d]	340
Field ramp rate at t_1	$dB/dt\|_{t_1}$	mT/s	51	280	484	153

[a]Cycle with Pb^{54+} lead ion beam; multiple injection for the LHC destination "NOMINAL".
[b]Cycle with proton beam; with single bunch for the LHC destination "LHCINDIV".
[c]Cycle with antiproton beam.
[d]The PS B-train has two markers, the second marker in the Focusing side trig at t_1=85 ms for a field $\bar{B}(t_1) = 48.5$ mT.

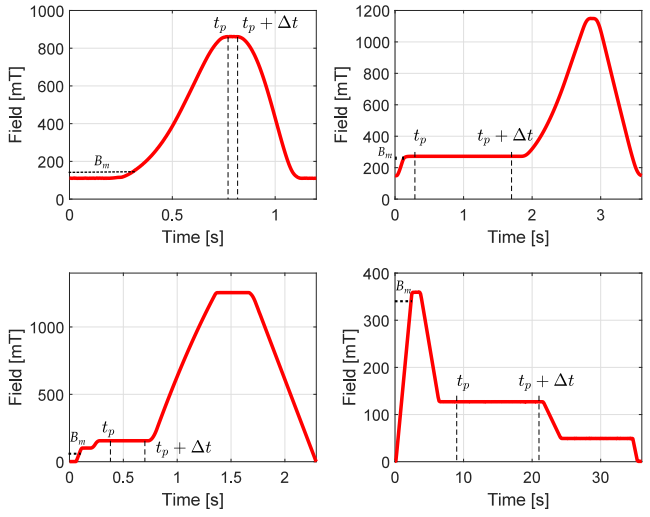

Fig. 3. PSB (top left), LEIR (top right), PS (bottom left) and ELENA (bottom right) commissioning cycles considered in this work. t_p refers to a plateau start time, Δt refers to the duration of the plateau and B_m refers to the field marker level.

LHC injector chain. Since these magnetic cycles vary widely in terms of the peak field reached, as well as other dynamic parameters, the results obtained include the confounding effects of magnetic hysteresis and therefore reflect the actual operating conditions.

While electronic, firmware and software components of the new B-train systems are uniform across all machines, some differences exist in the case of the sensor setup. These are linked to the characteristics of the magnetic cycles and to various practical constraints, which are described below.

2.3.1. PSB

The new PSB B-train system will become operational as of 2021. The tests described in this paper were carried out using a prototype version, including only one acquisition chain working in parallel with the legacy system. The sensors of both systems are installed in a reference magnet separate from the ring, excited in series with the bending dipoles. While the legacy system is based on a short induction coil, the new B-train is based on an integral coil with 1.6 m^2 equivalent surface that picks up the field, including in the end regions, which improves the accuracy of the measurement. In the end regions, the field is more affected by saturation and eddy current effects and has a different dynamic behavior. As a consequence, a direct comparison between the old and the new measurements, such as it was done for the initial calibration of the new B-train, may be affected by high uncertainty. The field marker setup is based on a NMR Metrolab teslameter PT2025 [22], including a probe marking at a field level of 110.8 mT, i.e., slightly lower than injection [23].

2.3.2. LEIR

LEIR is a comparatively small ring including four 90° bending dipoles, for which no spare unit was ever built. As a consequence, the sensors of both the legacy and new systems have been installed in the operating units. The legacy B-train is based on only one induction coil, sandwiched between the vacuum chamber and bottom magnet pole, so that maintenance or replacement are extremely impractical. Each chain of the new system includes a short 0.6 m^2 induction coil and a FMR field marker, installed next to each other in the non-uniform, fringe-field region [24] of the bending magnet. The marker is set at a field level of 251.2 mT, also slightly lower than injection.

2.3.3. PS

The PS ring includes 100 combined-function magnets, having hyperbolically-shaped poles that add a quadrupole field component to the dipole. In the two halves of the magnet the slope of the poles is inverted, so that the quadrupole is focusing in one and defocusing in the other. One additional magnet is powered in series and set aside as a reference for the B-train. Each half of the reference unit includes a short 1 m^2 induction coil, as well as an FMR field marker set to the level of 48.5 mT (focusing) or 49.5 mT (defocusing), i.e., just below injection. The slight difference between the two marker levels is due to the different field configuration in the two halves, and is aimed at having the two TTL triggers arriving approximately at the same time. The two halves function essentially as two independent magnets and the respective signals are fed in parallel to a single B-train acquisition chain, where the field values are averaged. In this study, performance statistics have been derived uniquely from the defocusing half, results from the other half being closely comparable.

2.3.4. ELENA

ELENA is the newest and smallest of CERN synchrotrons, as it consists of a ring with only six bending magnets that was completed in 2017. The setup used in the ELENA B-train consists of a separate reference magnet, in the gap of which there are an integral induction coil and two NMR markers per acquisition chain. The 2.9 m^2 coils are part of a 9-unit, litz-wire coil array that is curved to follow the strongly bent shape of the magnet [25]. As in the case of the PSB B-train, Metrolab PT2025 teslameters and NMR probes are used as part of the field marker setup. On each chain, a low-field marker is set at 45 mT, i.e., just below injection for commissioning cycles with proton acceleration, while a high-field marker is set at 340 mT, i.e. just before antiproton injection for operational deceleration cycles. For the purpose of this study, only the high-field marker has been considered.

3. Measurement error model

In general, the metrological capability of a measuring instrument can be determined by characterizing two components of measurement error. The first one, random error, causes inconsistencies in the repeatability of the measurement in the form of scatter, typically represented by the standard deviation, σ, of the measurand over a number of observations. The second component, the systematic error, causes a consistent difference between the measured and reference quantity values [26]. Considering the above definitions, the simplest model for defining the errors in B-trains is a linear, additive error model [27]:

$$\bar{B}(t) = (1 + \lambda)B(t) + \Delta B + \epsilon(t), \tag{2}$$

where $\bar{B}(t)$ refers to the measured and transmitted B-train output whilst $B(t)$ is the actual magnetic field, as seen by the beam. The three terms on the right-hand side represent three separate sources of errors. The first term with an error parameter λ, represents a systematic gain error

with typically $|\lambda| \ll 1$. The second term, ΔB, represents a systematic offset error. The third term, $\epsilon(t)$, indicates the random error. This is a function of time that can be represented by the sum of three uncorrelated contributions, which therefore add quadratically:

$$\epsilon(t) \approx \sqrt{\sigma_{\mathrm{d}}^2(t) + \sigma_{\mathrm{n}}^2 + \sigma_{\mathrm{m}}^2}, \tag{3}$$

where σ_{d} is the uncertainty in the field measurement due to integrator drift as a function of time, σ_{n} represents the uncertainty due to random noise and σ_{m} is the uncertainty associated to the field marker. These contributions are described in detail in the sections below, including the method by which they have been evaluated from experimental data. The results of this evaluation are listed in Table 2 for the four B-train systems.

4. Random error characterization

4.1. Integrator drift (σ_{d})

Integrator drift due to parasitic offset voltages is often the most significant error in inductive field measurements. Offset voltages can be viewed as the low-frequency component in the ubiquitous $1/f$ noise spectrum and may be caused by component imbalance in the electronics, thermoelectric effects or electromagnetic interference. B-train integrators implement several strategies for the reduction of drift, including a voltage source in series with the input, set manually via a potentiometer in order to cancel the input offset. Since the offset changes with time, periodic integrator reset as given by Eq. (1) is essential to prevent drift from accumulating from cycle to cycle; this would be catastrophic, considering that the integration may continue uninterrupted between maintenance stops for several months. Nevertheless, accumulation of drift during a single cycle can still be a problem, especially for longer cycles such as in ELENA, as shown in Fig. 4. This explains why the field marker should be made to trigger just before beam injection, when the accuracy required of the B-train measurement is most critical.

A practical way of estimating the drift consists in identifying a time interval $(t_{\mathrm{p}}, t_{\mathrm{p}} + \Delta t)$ during which the magnetic field is known *a priori* to be stable, due to the magnet excitation current $I(t)$ being kept constant ($\dot{I}(t) = 0$). As shown in Fig. 3, such field plateaus are generally available in most accelerator cycles, where they are used for beam injection, extraction or other purposes (e.g. electron cooling in ELENA). The start and end times of the plateaus must be adjusted to exclude any transients due to power converter instability or eddy current decay; having done so, they are usually well reproducible in subsequent cycles of the same type, which greatly simplifies automated post-processing. For a given cycle where a plateau has been identified, the drift rate $\dot{B}_{\mathrm{d}}$ in T/s can be evaluated, in the first approximation, as in Eq. (4):

$$\dot{B}_{\mathrm{d}} = \frac{\bar{B}(t_{\mathrm{p}} + \Delta t) - \bar{B}(t_{\mathrm{p}})}{\Delta t} - \left.\frac{B}{I}\right|_I \dot{I}, \tag{4}$$

where an appropriate correction is made for any excitation current drift, $\dot{I}$, scaled by the field-to-current ratio of the magnet evaluated at the appropriate current level. Taking into account additive noise, a more accurate evaluation can be obtained by computing a least-squares linear regression, according to the model in Eq. (5)

$$\tilde{B}(t) = \tilde{B}_0 + \left(\dot{B}_{\mathrm{d}} - \left.\frac{B}{I}\right|_I \dot{I}\right)(t - t_{\mathrm{p}}). \tag{5}$$

where $\tilde{B}(t)$ is the fitted magnetic field value, whilst $\tilde{B}_0$ is the fitted magnetic field value at $t = 0$. The average voltage offset that causes the observed field drift is given by:

$$V_0 = \dot{B}_{\mathrm{d}} A_{\mathrm{c}}. \tag{6}$$

On a given cycle, the offset can be taken with good approximation to be a constant, as it appears from the linear behavior of the field in Fig. 4; however, considerable, seemingly random variations are observed on time scales of several seconds and longer. This means that the measurement errors due to drift at different times during a cycle are strongly correlated, due to the (temporarily) systematic character of the offset; while instead, the error considered at an arbitrary time has a random character. To quantify this behavior, we first evaluate the RMS average of the observed drift over a set of N cycles:

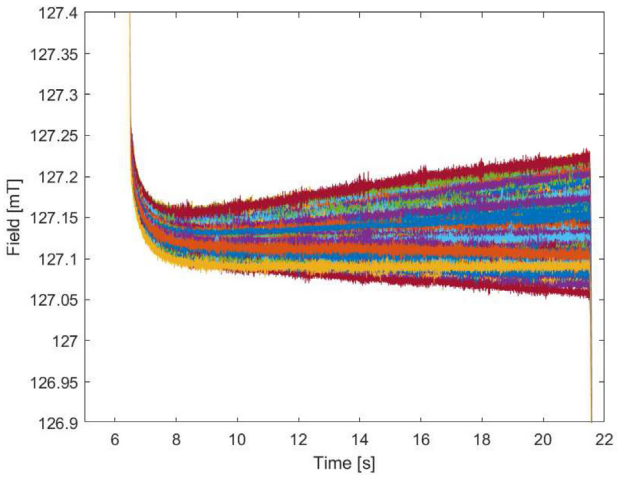

Fig. 4. Effect of drift on the measurement of ELENA's intermediate plateau (3000 observations).

$$\sigma\left(\dot{B}_{\mathrm{d}}\right) = \sqrt{\frac{1}{N}\sum_{k=1}^{N} \dot{B}_{\mathrm{d},k}^2} \tag{7}$$

and then we express the expected value of the field error as a function of time during a cycle as:

$$\sigma_{\mathrm{d}}(t) = \sigma\left(\dot{B}_{\mathrm{d}}\right)(t - t_k). \tag{8}$$

In all four B-train systems, the RMS coil voltage offset estimated from Eq. (6) is of the order of 20 μV or less. This is lower than the theoretical resolution of the digitized signals, which corresponds to 1 least significant bit of 76 μV for a typical ±10 V input range. The uncertainty of the estimated offset is inversely proportional to the square root of the number of samples included in the plateau considered, i.e. typically 2 or 3 orders of magnitude lower than the LSB. The maximum observed field drift does not exceed 20 μT/s, which is negligible for short cycles such as those in PSB, LEIR and PS. In ELENA the maximum drift observed is much lower, i.e., about 2 μT/s RMS, which can be attributed to careful tuning of the on-board offset-cancellation potentiometer (see Section 4.1). This operation is quite time-consuming, and was not carried out on the other systems in order to save beam time. In spite of such a good instrument performance, the drift in ELENA can still be a problem due to the duration of the plateaus needed for electron cooling, which are expected to last for up to two minutes. Alternative techniques to mitigate field errors in such cases are discussed in [28].

The evolution of the uncertainty associated to drift as a function of time is illustrated in Fig. 5, which shows the distribution of the field measured in ELENA at injection and extraction over 3000 consecutive cycles, normalized with respect to the respective averages. The standard deviation σ_{d} at extraction is about six times higher than at injection, which is however still within tolerance. The shape of the distributions is approximately gaussian, which confirms the essentially random nature of the voltage offset fluctuations over time.

4.2. Random noise (σ_{n})

The random noise represents the lowest-level error. This is also most easily evaluated on a plateau, as the RMS value of the residual of the

Table 2
Summary of performance indicators.

Parameter	Equation	Unit	PSB	LEIR	PS	ELENA
RMS coil voltage offset, V_0	(6)	μV	6	17	10	0.5
Drift rate, $\dot{B}_d$	(4)	μT/s	8.8 ± 3.1	9.2 ± 3.7	10 ± 10	1.0 ± 1.5
Random error due to drift at injection, $\sigma_d(t_{inj})$	(8)	μT	0.24	1.2	0.86	0.62
Random error due to drift at extraction, $\sigma_d(t_{ext})$	(8)	μT	1.89	25	16	42
Random error due to noise, σ_n	(9)	μT	7.7	15	1	2.9
Random error due to marker jitter, σ_m	(13)	μT	9.0	12	1.5	0.5
Total random error at injection, $\epsilon(t_{inj})$	(3)	μT	10.9	21.2	1.7	4.5
Total random error at extraction, $\epsilon(t_{ext})$	(3)	μT	11.0	32.8	16.0	42.2
Measured reproducibility at injection, $\sigma(\bar{B}(t_{inj}))$	–	μT	15	14	1.2	4.1
Measured reproducibility at extraction, $\sigma(\bar{B}(t_{ext}))$	–	μT	17	19	16	37
Systematic gain error, λ (before/after calibration)	(18)	ppm	−451/n.a.	−529/n.a.	67/n.a.	−2600/6.3
Systematic offset error, ΔB (before/after calibration)	(18)	μT	56/n.a.	190/n.a.	−18/n.a.	770/−1.3

linear regression equation in Eq. (5):

$$\sigma_n = \sqrt{\frac{1}{\Delta t}\int_{t_p}^{t_p+\Delta t} \left(\bar{B}(\tau) - \tilde{B}(\tau)\right)^2 d\tau}. \tag{9}$$

The measured noise levels are comparable with the uncertainty associated to integrator drift. The highest noise level, $\sigma_n = 15$ μT, is seen in LEIR, where it could be conceivably caused by the coil being fully exposed to external EM interference. The lowest level, $\sigma_n = 1$ μT, is seen in the PS, where the major differentiating characteristic is that the magnet power supply is controlled in closed-loop by the B-train feedback, thus providing extremely smooth plateaus. This suggests that Eq. (9) overestimates the noise, as it includes a contribution from power supply ripple. The noise levels declared here were calculated based on a measurement frequency of 10 kHz.

4.3. Field marker uncertainty (σ_m)

The error associated to the field marker can be characterized in terms of the delay between the time t_k when the field reaches the preset threshold value, i.e. $B(t_k) = B_m$, and the time $\tilde{t}_k$ when the TTL trigger is actually received by the integrator:

$$\Delta t_k = \tilde{t}_k - t_k > 0. \tag{10}$$

The delay Δt_k includes a dominant contribution from the systematic latency associated to the detection of the resonance and the generation of the trigger pulse, plus a random component. The latency is accounted for by the systematic offset term ΔB in Eq. (2). The principal sources of random errors contributing to σ_m are temperature fluctuations and, especially, mechanical and electrical noise, which has an impact on the differentiating algorithm used to identify the resonance peak in the sensor's output signal. The contribution associated to the frequency stability of the RF signal source is typically of the order of one ppm or better, which can be safely neglected. In the first approximation, the resulting field error is proportional to the delay:

$$B(t_k + \Delta t_k) - B(t_k) \approx \frac{dB}{dt}\Delta t_k. \tag{11}$$

Analogously to the case of integrator drift, this error has a systematic character for any given magnetic cycle, but on a cycle-to-cycle basis it should be considered as a random variable that can be interpreted as the jitter of the field marker. Experimentally, the delay Δt_k is not directly accessible since the true field B is unknown. An estimate, however, can be obtained under reproducibility conditions from the standard deviation of the trigger times measured over a sequence of N identical cycles:

$$\sigma(\Delta t)^2 \le \sigma(\tilde{t}_k)^2 = \frac{1}{N}\sum_{k=1}^{N}\tilde{t}_k^2 - \left(\frac{1}{N}\sum_{k=1}^{N}\tilde{t}_k\right)^2. \tag{12}$$

The inequality in Eq. (12) takes into account that ripple in the magnet excitation current may produce a slightly different field at the same time during a magnetic cycle, even when the cycles are nominally identical. As a result, we may take the upper bound as a conservative error estimate:

$$\sigma_m = \frac{dB}{dt}\sigma(\tilde{t}_k) \tag{13}$$

As reported in Table 2, this error component is also very low, of the order of a few microtesla, i.e. generally comparable to the noise level. The highest level, $\sigma_m = 12$ μT, is found again in LEIR, in all likelihood due to the external installation of the sensors.

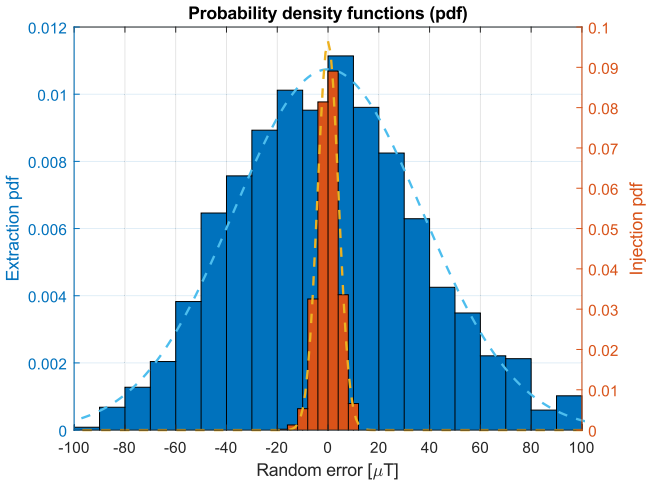

Fig. 5. Probability density functions (pdfs) of the ELENA random error measurement at injection (orange) and extraction (blue). (For interpretation of the references to color in this figure legend, the reader is referred to the web version of this article.)

4.4. Total random error $\epsilon(t)$

The total random error evaluated according to the model of Eq. (3) is given in Table 2 both at injection and at extraction. At injection, the dominant contribution is the noise σ_n. Even in the worst case, i.e., LEIR, the random error relative to the peak field is well below 20 ppm. At extraction the dominant contribution is the drift σ_d, except for the PSB due to the brief duration of the acceleration ramp. Even in the worst case, i.e., ELENA, the relative error is about 100 ppm, which is acceptable for operation.

These results should be compared to the actual reproducibility of the measured magnetic field $\bar{B}$, evaluated by taking the standard deviation over 3000 cycles as discussed in Section 2.3 and also given in Table 2. The RMS difference between the measured reproducibility and the estimated total random error is as low as 6 μT (17 ppm). This essentially validates the assumptions on which the model of Eq. (3) is based.

5. Systematic error evaluation and calibration

5.1. Beam-based calibration

In general, the systematic error of an instrument should be estimated either by measuring a metrological reference standard that realizes the measurand, or by comparing the measurements results to those obtained with another instrument, known to be more accurate. In our case, i.e. a dynamic magnetic field, there are no internationally accepted metrological standards or reference instruments, other than the kind of inductive setup we wish to calibrate. As a result, we performed an indirect calibration such as it is possible in the domain of synchrotrons, based upon measurements done on the circulating beam via the RF subsystem.

In a synchrotron, the RF varies during the acceleration ramp in order to keep the particles on the reference closed orbit. The accelerating electric field, provided by the RF cavity at the particle revolution frequency f_{rev}, is dependent on the magnetic field B provided by the main bending magnets. The frequency control strategy implemented in CERN's new Low-Level RF (LLRF) system [29] is represented schematically in Fig. 6. First, the field $\bar{B}(t)$ distributed by the B-train is used to compute the so-called frequency program, i.e., the theoretical revolution frequency of a particle on the reference closed orbit, according to the relationship [30,31]:

$$f_{\mathrm{prg}} = \frac{c}{2\pi R}\sqrt{1 - \frac{1}{1 + \left(\frac{\bar{B}\rho q}{m_0 c}\right)^2}} \tag{14}$$

where c is the speed of light in vacuum, the radical term is the relativistic β, R is the mean reference orbit radius, ρ is the bending radius, q is the particle's charge and m_0 is its rest mass. The frequency program of the four accelerators investigated is represented in Fig. 7. The frequency varies in the range from about 100 kHz to 1.5 MHz and is a monotonically increasing function of the field. In case of Pb^{54+} ion operation, the charge-to-mass ratio decreases by a factor ~4 and therefore the frequency also decreases, noticeably so in the PS at low field. As the particle momentum increases, β approaches unit value and the frequency ceases to vary appreciably with the field, as it can be seen for proton operation in the PS above about 0.2 T. The frequency applied to the cavity is obtained according to:

$$f_{\mathrm{rev}} = (f_{\mathrm{prg}} + f_{\mathrm{off}}) + f_{\mathrm{loops}} - f_{\mathrm{rad}}, \tag{15}$$

where:

- f_{off} is an optional frequency offset, defined in general as a function of field, added to f_{prg} in order to carry out special tests or to correct the B-train input when it is suspected to be wrong. During the present tests, f_{off} was set to zero.
- f_{loops} includes the contributions of three independent feedback loops: the longitudinal phase loop, which keeps the particles bunched together, and the injection and extraction loops, which synchronize the particle bunches in and out of the ring.
- f_{rad} is the radial loop contribution that keeps the beam in the center of the vacuum chamber. This loop is based on feedback from the mean radial position error δR, obtained by averaging the measurements of several transverse pick-up units (TPU) placed along the ring [32]. The minus sign in Eq. (15) is in accord with a polarity convention that associates a positive correction, $f_{\mathrm{rad}} > 0$, with a decrease in revolution frequency, as needed to push the beam radially outwards according to Eq. (14).

If we consider only the radial equilibrium (that is, if we ignore f_{loops}) in presence of a field measurement error δB, such that $B = \bar{B} + \delta B$, we have:

$$f_{\mathrm{rev}}(\bar{B} + \delta B) = f_{\mathrm{prg}} - f_{\mathrm{rad}}, \tag{16}$$

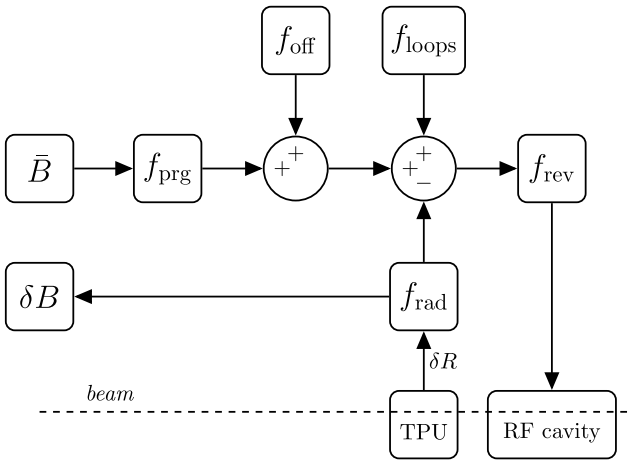

Fig. 6. Simplified schematic diagram of the Low-Level RF system (from [29]).

which means that, in the first approximation, the field error is proportional to the radial loop contribution f_{rad}:

$$\delta B = \bar{B} - B \approx \frac{f_{\mathrm{rad}}}{\frac{\partial f_{\mathrm{prg}}}{\partial B}}. \tag{17}$$

Attributing entirely δB to a B-train measurement error is a conservative hypothesis, as in reality the centering action of f_{rad} compensates also other perturbations such as environmental and stray magnetic fields, imperfect knowledge of the radius of the machine, and measurement errors of the beam radial position or the RF frequency. The term $(\partial f/\partial B)^{-1}$ in Eq. (17), expressed in μT/Hz, represents the uncertainty of the estimated field error per unit of uncertainty of the revolution frequency, and is also plotted in Fig. 7. We recall that the typical uncertainty of the frequency is 1 Hz or less. In general, the uncertainty ratio increases with the field, which means that field error estimates are generally more precise at injection than extraction (note that the field levels are inverted for antiproton decelerator operation in ELENA). The increase is limited to about one order of magnitude in PSB, LEIR and ELENA, but grows to as much as three orders of magnitude in the PS; as a result, the uncertainty of Eq. (17) must be evaluated very carefully at high field, as one might have expected considering that the frequency changes very little with the field. In view of future commissioning tests, we remark that this problem would be exacerbated by three orders of magnitude in the SPS, where both proton and ion beams are fully relativistic and the revolution frequency is practically constant. On the other hand, we observe that ion operation in the PS lowers the uncertainty at high field by one order of magnitude, due to the lower charge-to-mass ratio.

The field error in Eq. (17) can be evaluated at several different field levels over a set of repeated cycles, to obtain a set of N data points $(\bar{B}, \delta B)_n$, for $n \in [1, N]$. The systematic error parameters λ and ΔB defined in Eq. (2) can be estimated by least-square fitting the data points with the linear model:

$$\delta B = \lambda \bar{B} + \Delta B \tag{18}$$

obtained by substituting Eq. (17) in Eq. (2), neglecting the random error term and taking into account that both parameters are small. The quality of the results obtained may be affected by the higher uncertainty of δB values obtained at high field, due to the combination of higher uncertainty ratio $(\partial f/\partial B)^{-1}$ and integrator drift from Eq. (8). As a consequence, the accuracy of the estimated gain error parameter λ must be expected in general to be lower than the accuracy of the offset ΔB.

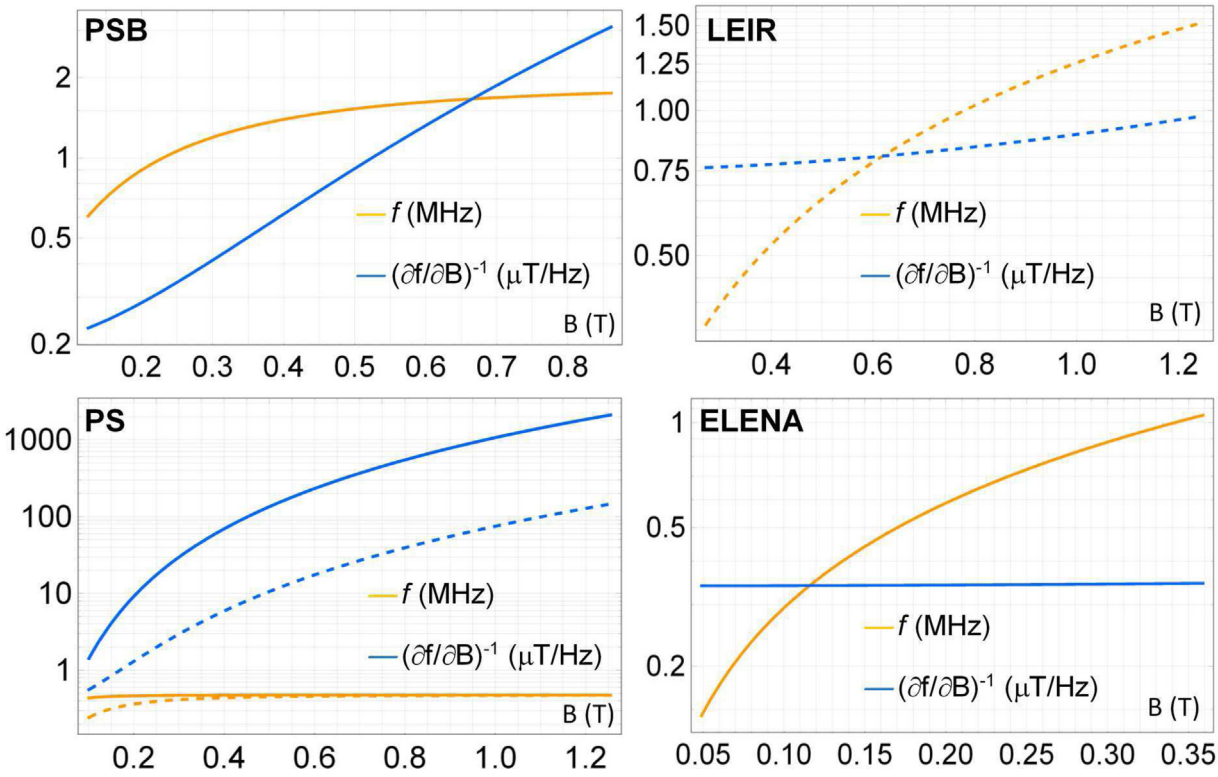

Fig. 7. The revolution frequency (orange) and its the reciprocal of its first derivative (blue) as a function of the magnetic field for PSB, LEIR, PS and ELENA. The continuous lines refer to proton or antiproton beams, while the dotted lines to Pb^{54+} ion operation. (For interpretation of the references to color in this figure legend, the reader is referred to the web version of this article.)

5.2. Experimental results

The results of the beam-based calibration campaign carried out for the four B-train systems are listed in Table 2. The original calibration parameters were obtained from a comparison with the legacy B-train systems in the case of LEIR, PS and PSB, while instead the ELENA system was setup according to the *ab initio* measurement model detailed in Ref. [33]. The PS is the only system with systematic errors fully below the desired tolerance, thanks to extensive fine-tuning carried out during several years of operation of the prototype system. The higher gain errors in the PSB and LEIR, which are of the order of 0.05%, can be ascribed to the differences between the induction coils in the new and legacy systems, as discussed in Section 2.3. The large initial gain error in ELENA, about −0.26%, may be attributed to the difference between the magnets in the ring and the reference unit, which was made with a different grade of magnetic steel. In all cases, however, the resulting radial position error remained well within the correction capabilities of the radial loop and stable beam operation was routinely achieved.

The calibrated parameters λ and ΔB can be easily applied as incremental corrections into the B-train acquisition chain. In the PSB, LEIR and PS this was not done, in order not to perturb operation of the LHC injector chain prior to the impending shutdown. Instead, the ELENA system was calibrated and the beam-based test was repeated. Measurements were acquired repeatedly when the RF is on, as shown in Fig. 8 for the ELENA cycle as an example. The field error values δB measured before and after calibration are plotted in Fig. 9. The calibration reduces both gain and offset errors by more than two orders of magnitude, down to the level of just a few ppm, i.e. well below random errors. The soundness of this procedure was further verified by showing that, even with the radial RF loop switched off, the beam could be still injected and extracted with minimal losses.

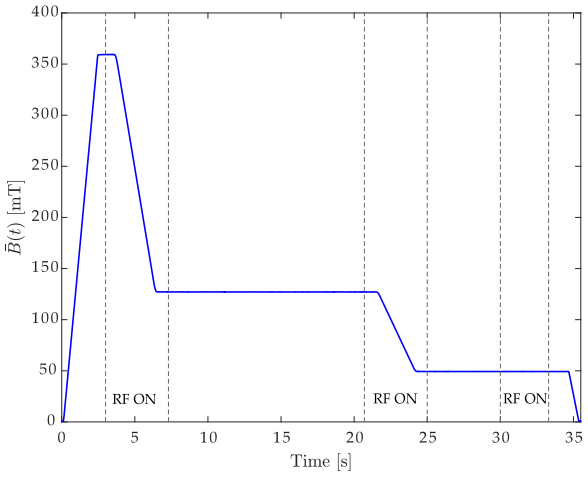

Fig. 8. The points in the ELENA cycle where RF is on and measurements were acquired.

6. Conclusions

In this work, we reported on the performance of the new FIRESTORM B-train systems developed at CERN for real-time magnetic field measurement in the PSB, PS, LEIR and ELENA synchrotrons. During an extensive series of preliminary tests, all systems allowed smooth and reliable beam operation, thus proving their viability for the restart of the accelerator complex in 2021. Their metrological performance was evaluated conservatively, using a model that characterizes random and systematic errors separately.

The worst-case random errors range from 20 ppm at injection to about 100 ppm at extraction, which are lower figures than in the legacy B-train systems. Random errors at injection are dominated by noise,

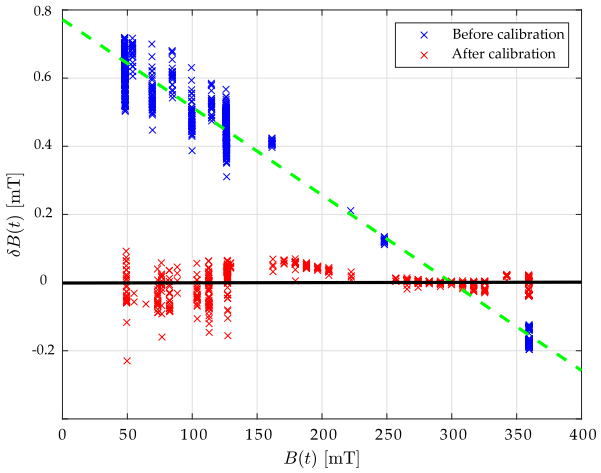

Fig. 9. $B(t)$ vs. $\delta B(t)$ before and after the ELENA B-train's calibration.

which is intrinsic to the system and hard to abate. At extraction, on the other hand, the dominant contribution is integrator drift, which can be reduced using a variety of different techniques.

Systematic errors were calibrated by means of a novel procedure, using beam-based measurements. The systematic component of the model is fitted with the least-squares method to measurements of the field error δB, estimated from the RF frequency correction associated to the radial feedback loop, f_{rad}. This way of proceeding is straightforward, since the necessary signals are readily made available for every magnetic cycle by the distributed accelerator control infrastructure. It would be possible, in principle, to directly use the mean radial beam position error δR to infer δB, achieving better accuracy. However, doing so requires the radial RF loop to be switched off, which can be done only sporadically during dedicated test (a.k.a. "Machine Development") sessions.

In ELENA, the calibration procedure based on f_{rad} reduced systematic errors by two orders of magnitude, down to the level of a few ppm. The original calibration of the ELENA system was done following an *ab initio* concept [33], based on the availability of a full set of magnetic measurements for all magnetic units. However, the reference magnet is different from the others in terms of its response to excitation history, due to dynamic effects and magnetic hysteresis, leading to initial systematic errors as high as 0.3%. This problem is exacerbated in the other, older machines, for which the magnetic measurement record is incomplete. As a consequence, beam-based calibration appears to be always necessary.

The accuracy that can be obtained improves at low field levels, and (whenever applicable) with ion rather than proton beams. During the upcoming restart, we shall apply to PSB, LEIR and PS the systematic error coefficients listed in Table 2 and verify their viability for the whole set of magnetic cycles foreseen in operation. Extension of the method to the SPS might be attempted, but due to the very low sensitivity of the revolution frequency respect to the field the final, the expected accuracy is low.

Possible future improvements to the B-train's performance are being considered, such as an adapted field marker for drift correction on very long plateaus such as in ELENA [34], as well as monitoring and compensation of temperature effects. During the upcoming three-year operation phase, accumulation of δB and f_{rad} data is expected to provide the basis for high-precision statistical estimation of the calibration parameters and their stability.

CRediT authorship contribution statement

Christian Grech: Conceptualization, Methodology, Formal analysis, Investigation, Data curation, Writing - original draft. **Maria Amodeo:** Formal analysis, Investigation, Software, Validation. **Anthony Beaumont:** Methodology, Formal analysis, Investigation, Data curation, Writing - review & editing. **Marco Buzio:** Supervision, Project administration, Conceptualization, Methodology, Data curation, Writing - review & editing. **Vincenzo Di Capua:** Formal analysis, Investigation, Software, Validation. **David Giloteaux:** Methodology, Resources, Software, Validation. **Nicholas Sammut:** Supervision, Project administration, Conceptualization, Methodology, Writing - review & editing. **Joseph Vella Wallbank:** Methodology, Formal analysis, Investigation, Data curation, Writing - review & editing.

Declaration of competing interest

The authors declare that they have no known competing financial interests or personal relationships that could have appeared to influence the work reported in this paper.

Acknowledgments

The authors would like to thank CERN colleagues Martino Colciago and Marco Roda for their contribution to the B-train system, as well as Simon Albright, Maria Elena Angoletta, Christian Carli, Heiko Damerau, Alan Findlay, Michael Jaussi, and Damien Perrelet for their essential contribution towards acquisition and interpretation of the Low-Level RF measurements. The publication fee was funded by CERN.

References

[1] P. Bryant, K. Johnsen, The Principles of Circular Accelerators and Storage Rings, Cambridge University Press, 2005, URL: https://books.google.ch/books?id=eU7EJkYTiNEC.

[2] Y. Tian, B. Oerter, An upgrade to of the magnet-field-driven timing systems at the AGS, ICALEPCS (2005).

[3] G. Franzini, O. Coiro, D. Pellegrini, M. Serio, A. Stella, M. Pezzetta, M. Pullia, Final design and features of the B-train system of CNAO, in: IPAC, IPAC, Kyoto, 2010, URL: http://accelconf.web.cern.ch/AccelConf/IPAC10/papers/wepeb079.pdf.

[4] M. Pezzetta, G. Bazzano, E. Bressi, L. Falbo, M. Pullia, C. Priano, O. Coiro, G. Franzini, D. Pellegrini, M. Serio, A. Stella, G. Venchi, B-train performances at CNAO, in: IPAC2011, San Sebastian, Spain, 2011, URL: https://accelconf.web.cern.ch/accelconf/IPAC2011/papers/mopo039.pdf.

[5] F. Osmic, M. Benedikt, A. Koschik, P. Urschütz, Status of medaustron – The Austrian ion therapy and research centre, in: Proceedings of the 5th Int. Particle Accelerator Conf. IPAC2014, 2014, p. WEPRO081.

[6] P. Fraboulet, K. Ambrosch, I.D. Cesaris, A. Beuret, The current and field regulation system of the medaustron ion-beam accelerator, in: IECON 2013 - 39th Annual Conference of the IEEE Industrial Electronics Society, IEEE, 2013, pp. 7103–7108, http://dx.doi.org/10.1109/iecon.2013.6700312.

[7] E. Feldmeier, R. Cee, M. Galonska, T. Haberer, A. Peters, S. Scheloske, The first magnetic field control (b-train) to optimize the duty cycle of a synchrotron in clinical operation, in: Conf. Proc., Vol. C1205201, 2012, pp. 3503–3505.

[8] E. Feldmeier, T. Haberer, A. Peters, C. Schoemers, R. Steiner, Magnetic field correction in normal conducting synchrotrons, in: IPAC, IPAC, Kyoto, 2010, URL: http://accelconf.web.cern.ch/AccelConf/IPAC10/papers/mopd004.pdf.

[9] M. Buzio, P. Galbraith, S. Gilardoni, D. Giloteaux, G. Golluccio, C. Petrone, L. Walckiers, Development of upgraded magnetic instrumentation for cern's real-time reference field measurement systems, in: IPAC, IPAC, Kyoto, 2010, URL: http://accelconf.web.cern.ch/AccelConf/IPAC10/papers/MOPEB016.pdf.

[10] C. Grech, A. Beaumont, M. Buzio, N. Sammut, Performance comparison of nuclear magnetic resonance and ferrimagnetic resonance field markers for the control of low-energy synchrotrons, J. Phys. Conf. Ser. 1065 (5) (2018) 052022.

[11] P. Di Cesare, C. Reymond, H. Rottstock, P. Sommer, SPS magnetic field cycle measurement system: Investigation on Nuclear Magnetic Resonnance (NMR) system to get a faster reading of field values, TechReport CERN-SPS-PCO-Note 89-9, CERN, Geneva, 1989, URL: https://cds.cern.ch/record/2158783.

[12] H. Kuhn, J.D. Pahud, The control systems for the CERN super proton synchrotron ring power supplies, IEEE Trans. Nucl. Sci. 28 (3) (1981) 3102–3104.

[13] D. Schoerling, Case study of a magnetic system for low-energy machines, Phys. Rev. Accel. Beams 19 (2016) 082401.

[14] E. Mobs, The CERN accelerator complex - august 2018, 2019, URL: https://cds.cern.ch/record/2684277 General Photo.

[15] L. Bottura, K.N. Henrichsen, Field measurements, in: CAS - CERN Accelerator School on Superconductivity and Cryogenics for Accelerators and Detectors, CERN-LHC-2002-020-MTA, CERN, Geneva, 2002, pp. 118–148, http://dx.doi.org/10.5170/CERN-2004-008.118, URL: https://cds.cern.ch/record/597621.

[16] Xilinx, Spartan 6 FPGA, Xilinx, 2011, https://www.xilinx.com/support/documentation/data_sheets/ds160.pdf.
[17] CERN, Simple PCIe FMC carrier (SPEC), CERN, 2010, https://www.ohwr.org/project/spec/wikis/home.
[18] M. Benedikt, F. Caspers, T. Salvermoser, Absolute Calibration of the CERN PS-Booster Bending Field with Beam and NMR, TechReport PS-OP-Note-98-23, CERN, Geneva, 1998.
[19] A. Beaumont, M. Buzio, G. Boero, Ferrimagnetic resonance field sensors for particle accelerators, Rev. Sci. Instrum. 90 (6) (2019).
[20] P. Jansweijer, H. Peek, E. de Wolf, White rabbit: Sub-nanosecond timing over ethernet, Nucl. Instrum. Methods Phys. Res. A 725 (2013) 187–190.
[21] T. Hoffmann, FESA Primer, Technical Report, GSI, Geneva, 2007, URL: https://wiki.gsi.de/foswiki/pub/Personalpages/FESA/FESAPrimer_TH.pdf.
[22] METROLAB, PT2025 NMR Teslameter User Manual, second ed., METROLAB Instruments SA, Geneva, Switzerland, 2003, URL: https://www.metrolab.com/wp-content/uploads/2015/07/PT2025_user_manual.pdf.
[23] C. Grech, R. Avramidou, A. Beaumont, M. Buzio, N. Sammut, J. Tinembart, Metrological characterization of nuclear magnetic resonance markers for real-time field control of the CERN ELENA ring dipoles, IEEE Sens. J. 18 (14) (2018) 5826–5833.
[24] S. Albright, R.A. Fernández, M.E. Angoletta, H. Bartosik, A. Beaumont, G. Bellodi, N. Biancacci, M. Bozzolan, M. Buzio, F.D. Lorenzo, A. Frassier, D. Gamba, S. Hirlander, A. Huschauer, S. Jensen, V. Kain, G. Kotzian, D. Kuchler, A. Latina, T. Levens, E. Mahner, E. Manosperti, O. Marqversen, D. Nicosia, M. O'Neil, E. Ozturk, A.S. Hernandez, R. Scrivens, G. Tranquille, F.J.C. Wenander, C. Wetton, M. Zampetakis, Review of the LEIR operation in 2018, 2020, AST note.
[25] O. Dunkel, Measurement methods and devices for curved dipole and combined function magnets, in: IMMW19, CERN, 2015, URL: https://edms.cern.ch/document/1559097/1.
[26] L. Mari, A. Giordani, Modeling measurement: Error and uncertainty, in: M. Boumans, G. Hon, A. Petersen (Eds.), Error and Uncertainty in Scientific Practice, Pickering & Chatto, 2014, pp. 79–96.
[27] Y. Tian, G.S. Nearing, C.D. Peters-Lidard, K.W. Harrison, L. Tang, Performance metrics, error modeling, and uncertainty quantification, Mon. Weather Rev. 144 (2) (2016) 607–613.
[28] M. Amodeo, P. Arpaia, M. Buzio, Integrator drift compensation of magnetic flux transducers by feed-forward correction, Sensors 19 (24) (2019) 5455.
[29] M.E. Angoletta, S. Albright, S. Energico, S. Hancock, M. Jaussi, A. Jones, J. Molendijk, M. Paoluzzi, J. Sanchez-Quesada, Initial beam results of CERN elena's digital low-level RF system, in: IPAC2017, CERN-ACC-2017-264, Copenhagen, Denmark, 2017, THPAB142, http://dx.doi.org/10.18429/JACoW-IPAC2017-THPAB142, 4 p. URL: https://cds.cern.ch/record/2289141.
[30] C. Bovet, R. Gouiran, I. Gumowski, K.H. Reich, A Selection of Formulae and Data Useful for the Design of A.G. Synchrotrons, CERN, Geneva, 1970, URL: https://cds.cern.ch/record/104153?ln=en.
[31] P. Baudrenghien, Low-level RF - part i: Longitudinal dynamics and beam-based loops in synchrotrons, 2012, p. 27 p, Comments: 27 pages, contribution to the CAS - CERN Accelerator School: Specialised Course on RF for Accelerators; 8 - 17 Jun 2010, Ebeltoft, Denmark.
[32] R. Marco-Hernández, D. Alves, M.E. Angoletta, O. Marqversen, J. Molendijk, E. Oponowicz, R. Ruffieux, J. Sánchez-Quesada, L. Søby, The AD and ELENA orbit, trajectory and intensity measurement systems, JINST 12 (07) (2017).
[33] C. Grech, M. Buzio, N. Sammut, A magnetic measurement model for real-time control of synchrotrons, IEEE Trans. Instrum. Meas. (2019).
[34] M. Amodeo, Metrological Characterization of Field Markers for Real-Time Measurement and Control of Accelerator Magnets (Master's thesis), University of Naples Federico II, 2018.